arXiv:1611.06097v1 [math.NA] 29 Oct 2016

Reduced Order Modeling for Heston Stochastic Volatility Model

Bülent Karasözen[a,b], Sinem Kozpınar[a], Murat Uzunca[a], Yeliz Yolcu Okur[a]

[a] *Institute of Applied Mathematics, Middle East Technical University, 06800 Ankara, Turkey*
[b] *Department of Mathematics, Middle East Technical University, 06800 Ankara, Turkey*

Abstract

In this paper we compare two model order reduction techniques, the Proper Orthogonal Decomposition (POD) and Dynamic Mode Decomposition (DMD), for Heston's option pricing model. The full order model is obtained by discontinuous Galerkin discretization in space and backward Euler in time. Numerical results for butterfly spread, European and digital call options reveal that in general DMD requires more modes than the POD modes as expected at the same level of accuracy. However, the speed-up factors are much higher for DMD than POD due to the equation free nature of the DMD.

Keywords: Option pricing, Heston model, discontinuous Galerkin method, reduced order modeling, proper orthogonal decomposition, dynamic mode decomposition
2000 MSC: 65M60, 91B25, 91G80

1. Introduction

Under Heston framework [12], the volatility is treated as a square root process which enables us to predict the volatility smirk arising in the option prices. As a result one can obtain more accurate prices for the European currency options. One of the well-known techniques to solve option pricing problems is the Monte Carlo integration. Although its implementation is straightforward, it requires large number of realizations to achieve high accuracy. Moreover, one can estimate only one option price for a given underlying value. Therefore, the simulations can be too costly which leads us to the discretization methods based on the solution of partial differential equations (PDEs). Option pricing problems under Heston model are also represented as diffusion-convection-reaction PDEs [12, 19]. The diffusion matrix and convective field depend on the volatility. The diffusion matrix contains cross-diffusion terms as a result of the correlation

Email addresses: bulent@metu.edu.tr (Bülent Karasözen), ksinem@metu.edu.tr (Sinem Kozpınar), uzunca@gmail.com (Murat Uzunca), yyolcu@metu.edu.tr (Yeliz Yolcu Okur)

between the volatility and the underlying security price. In addition, the initial and boundary data is discontinuous and less regular for different options. Heston's PDE is solved in the literature by finite differences [13, 27, 8] and by finite elements [31]. Recently the authors [16] applied discontinuous Galerkin (dG) method to the Heston's PDE. The discontinuous Galerkin finite element (dGFEM) method has several advantages over finite difference and continuous finite element methods for solving diffusion-convection-reaction equations. Because the dGFEM does not require continuity across the inter-element boundaries, the number of degrees of freedom is larger than the continuous FEMs. On the other hand, the dGFEM has a number of desirable properties like the treatment of the convective term by upwinding, weakly enforcement of the boundary conditions, ease of parallelization.

In the last two decades the reduced order modeling became an important tool for simulating engineering problems efficiently. Reduced order models (ROMs) reduce the computational complexity and time by approximatating the full order model (FOM) of the high dimensional discretized partial differential equations (PDEs) as lower dimensional models. This enables fast simulation based studies like calibration and hedging [6, 10, 23, 25] in option pricing. In this paper we compare two model order reduction (MOR) methods, the proper orthogonal decomposition (POD) and dynamic mode decomposition (DMD) for Heston's option pricing model. The POD is the most known and frequently used reduced order modelling method. POD based reduced order modeling is investigated for pricing European and American options under Black-Scholes and Heston model [4, 21, 22]. Reduced-order models based on POD are optimal in terms of energy content. The energy content is important but is not sufficient in general to catch the dynamical behavior. In this paper we apply first time the recently emerged MOR technique, the DMD [26, 29] for option pricing and compare with the POD with respect to accuracy and speed-up over the full order models. The DMD is able to extract dynamically relevant flow features from time-resolved experimental or numerical data by generalizing the global stability modes and approximating the eigenvalues and eigenfunctions of the Koopman operator [15]. Both methods use the snapshots of the fully discretized PDEs in time. The POD solves a low dimensional model by Galerkin projection, whereas DMD is equation free, the reduced solution is given in form of Fourier series in time and space. We would like to remark that due to its computational efficiency, the DMD is used for financial applications like in high frequency trading [20] and stock market data analysis [7].

The paper is organized as follows: In the next section, Section 2, we give the full order model (FOM) of the Heston's PDE applying dG discretization in space and backward Euler discretization in time. In Section 3, the reduced order modeling of Heston's PDE by POD and DMD is described. In the last section, Section 4, we present numerical results for the butterfly spread, European call and digital options by comparing the POD and DMD reduced solutions with respect to accuracy and speed-up. The paper ends with some conclusions.

2. Full order model

2.1. Heston model as diffusion-convection-reaction equation

The Heston model can be characterized by a two-dimensional diffusion-convection-reaction equation with variable coefficients. Let $u^S(t, v_t, S_t)$ be the value of a European option with the underlying price S_t and volatilty v_t and let $g(v_T, S_T)$ denote the payoff received at maturity T. Then, the option price $u^S(t, v_t, S_t)$ under Heston model satisfies the following linear two-dimensional variable coefficient diffusion-convection-reaction equation [12]

$$\frac{\partial u^S}{\partial t} + \mathcal{J}_t^S u^S - r_d u^S = 0, \tag{1}$$

with the terminal condition

$$u^S(T, v_T, S_T) = g(v_T, S_T),$$

where $v_t > 0$, $S_t > 0$, $t \in [0, T]$, and

$$\mathcal{J}_t^S u^S = \frac{1}{2} S^2 v \frac{\partial^2 u^S}{\partial S^2} + (r_d - r_f) S \frac{\partial u^S}{\partial S} + \rho\sigma S v \frac{\partial^2 u^S}{\partial v \partial S} + \frac{1}{2}\sigma^2 v \frac{\partial^2 u^S}{\partial v^2} + \kappa(\theta - v)\frac{\partial u^S}{\partial v}.$$

Here, r_d is the domestic interest rate, r_f is the foreign interest rate, θ is the long-run mean level of v_t, σ is the volatility of the volatilty and ρ is the correlation coefficient. Applying the so called log transformation $x = \log(S/K)$ and $\tau = T - t$ with $u(\tau, v, x) = u^S(T - \tau, v, Ke^x)$, PDE (1) is converted to the following equation

$$\frac{\partial u}{\partial \tau} - \mathcal{J}_\tau^x u + r_d u = 0, \tag{2}$$

where $v > 0$, $x \in (-\infty, \infty)$, $\tau \in [0, T]$, and

$$\mathcal{J}_\tau^x u = \frac{1}{2} v \frac{\partial^2 u}{\partial x^2} + (r_d - r_f - \frac{1}{2} v)\frac{\partial u}{\partial x} + \rho\sigma v \frac{\partial^2 u}{\partial v \partial x} + \frac{1}{2}\sigma^2 v \frac{\partial^2 u}{\partial v^2} + \kappa(\theta - v)\frac{\partial u}{\partial v}.$$

Note that due to the substitution $\tau = T - t$, PDE (2) can also be regarded as a forward equation with the following initial condition

$$u^0 := u(0, v, x) = g(v, Ke^x).$$

We consider an open bounded domain Ω with the boundary $\Gamma = \Gamma_D \cup \Gamma_N$, where on Γ_D the Dirichlet and on Γ_N the Neumann boundary conditions are prescribed, respectively. Then, the log transformed PDE given in (2) is expressed as a diffusion-convection-reaction equation

$$\frac{\partial u}{\partial \tau} - \nabla \cdot (A \nabla u) + b \cdot \nabla u + r_d u = 0 \qquad \text{in } (0, T] \times \Omega, \tag{3a}$$

$$u(t, \boldsymbol{z}) = u^D(t, \boldsymbol{z}) \qquad \text{on } (0, T] \times \Gamma_D, \tag{3b}$$

$$A \nabla u(t, \boldsymbol{z}) \cdot \boldsymbol{n} = u^N(t, \boldsymbol{z}) \qquad \text{on } (0, T] \times \Gamma_N, \tag{3c}$$

$$u(0, \boldsymbol{z}) = u^0(\boldsymbol{z}) \qquad \text{in } \{0\} \times \Omega, \tag{3d}$$

where $\boldsymbol{n}$ is the outward unit normal vector, $\boldsymbol{z} = (v, x)^T$, throughout this paper, denotes the spatial coordinates. In (3), the diffusion matrix and convective field are given by

$$A = \frac{1}{2} v \begin{pmatrix} \sigma^2 & \rho\sigma \\ \rho\sigma & 1 \end{pmatrix} \quad \text{and} \quad b = v \begin{pmatrix} \kappa \\ \frac{1}{2} \end{pmatrix} + \begin{pmatrix} -\kappa\theta + \frac{1}{2}\sigma^2 \\ -(r_d - r_f) + \frac{1}{2}\rho\sigma \end{pmatrix}.$$

Remark 1. *Although, the transformed PDE (2) is defined on the computational domain $(0, \infty) \times (-\infty, \infty)$, dGFEM must be performed on a bounded spatial region $\Omega = (v_{min}, v_{max},) \times (x_{min}, x_{max})$ for the numerical simulations, which is known as localization in option pricing models.*

2.2. Variational form of Heston's model

We introduce the weak formulation of Heston's model as parabolic convection-diffusion-reaction equation (3a-3d). Let $L^2(\Omega)$ be the space consisting of all square integrable functions on Ω, $H^1(\Omega)$ denote the Hilbert space of all functions having square integrable first-order partial derivatives, and $H_0^1(\Omega) = \{w \in H^1(\Omega) : w = 0 \text{ on } \Gamma_D\}$. The weak form of (3) is obtained by multiplying with a test function $w \in H_0^1(\Omega)$ and integrating by parts over the domain Ω. Then, for a.e. $t \in (0, T]$, we seek a solution $u(t, v, x) \in H_D^1(\Omega) = \{w \in H^1(\Omega) : w = u^D \text{ on } \Gamma_D\}$ satisfying

$$\int_\Omega \frac{\partial u}{\partial \tau} w d\boldsymbol{z} + a(u, w) = \int_{\Gamma_N} u^N w ds \qquad \forall w \in H_0^1(\Omega), \tag{4a}$$

$$\int_\Omega u(0, \boldsymbol{z}) w d\boldsymbol{z} = \int_\Omega u^0 w d\boldsymbol{z} \qquad \forall w \in H_0^1(\Omega), \tag{4b}$$

where ds is the arc-length element on the boundary. In (4a-4b), $a(u, w)$ is the bilinear form given by

$$a(u, w) = \int_\Omega \left(A\nabla u \cdot \nabla w + b \cdot \nabla u w + r_d u w\right) d\boldsymbol{z}, \quad \forall w \in H_0^1(\Omega).$$

We assume that the matrix A is positive definite for $v > 0$ and $\rho \in (-1, 1)$ which is usually satisfied.

2.3. Discontinuous Galerkin discretization in space

The symmetric interior penalty Galerkin (SIPG) method is the commonly used dG method, which enforces boundary conditions weakly [24]. Let the mesh $\xi_h = \{K\}$ be a partition of the domain Ω into a family of shape regular elements (triangles). We set the mesh-dependent finite dimensional solution and test function space by

$$W_h = W_h(\xi_h) = \left\{w \in L^2(\Omega) : w|_K \in \mathbb{P}_k(K),\ \forall K \in \xi_h\right\} \not\subset H_0^1(\Omega),$$

where the functions in W_h are discontinuous along the inter-element boundaries. These discontinuities leads to the fact that on an interior edge e shared by two

neighboring triangles K_i and K_j, there are two different traces from either triangles. Thus, for the convenience, we define the jump and average operators of a function $w \in W_h$ on e by

$$[\![w]\!] := w|_{K_i}\boldsymbol{n}_{K_i} + w|_{K_j}\boldsymbol{n}_{K_j}\ , \quad \{\!\{w\}\!\} := \frac{1}{2}(w|_{K_i} + w|_{K_j}).$$

On a boundary edge $e \subset \partial\Omega$, we set $[\![w]\!] := w|_K\boldsymbol{n}$ and $\{\!\{w\}\!\} := w|_K$. In addition, we form the sets of inflow and outflow edges by

$$\Gamma^- = \{\boldsymbol{z} \in \partial\Omega : \boldsymbol{b}(v)\cdot\boldsymbol{n}(v,x) < 0\}\ , \qquad \Gamma^+ = \partial\Omega \setminus \Gamma^-,$$
$$\partial K^- = \{\boldsymbol{z} \in \partial K : \boldsymbol{b}(v)\cdot\boldsymbol{n}_K(v,x) < 0\}\ , \qquad \partial K^+ = \partial K \setminus \partial K^-,$$

where $\boldsymbol{n}_K$ denotes the outward unit vector on an element boundary ∂K. Moreover, we denote by Γ_h^0 and Γ_h^D the sets of interior and Dirichlet boundary edges, respectively, so that the union set is $\Gamma_h = \Gamma_h^0 \cup \Gamma_h^D$. Then, in space SIPG discretized semi-discrete system of the PDE (3) reads as: for a.e. $t \in (0,T]$, for all $w_h \in W_h$, find $u_h := u_h(t,\boldsymbol{z}) \in W_h$ such that

$$\int_\Omega \frac{\partial u_h}{\partial t} w_h d\boldsymbol{z} + a_h(t;u_h,w_h) = l_h(w_h), \tag{5a}$$
$$\int_\Omega u_h(0,\boldsymbol{z}) w_h d\boldsymbol{z} = \int_\Omega u^0 w_h d\boldsymbol{z}, \tag{5b}$$

with the (bi)linear forms:

$$\begin{aligned}
a_h(t;u_h,w_h) = &\sum_{K\in\xi_h}\int_K (A\nabla u_h\cdot\nabla w_h + b\cdot\nabla u_h w_h + r_d u_h w_h)\, d\boldsymbol{z} \\
&+ \sum_{e\in\Gamma_h}\int_e \left(\frac{\sigma_e}{h_e}[\![u_h]\!]\cdot[\![w_h]\!] - \{\!\{A\nabla w_h\}\!\}[\![u_h]\!] - \{\!\{A\nabla u_h\}\!\}[\![w_h]\!]\right) ds \\
&+ \sum_{K\in\xi_h}\left(\int_{\partial K^-\setminus\partial\Omega} b\cdot\boldsymbol{n}_K(u_h^{out}-u_h)w_h ds - \int_{\partial K^-\cap\Gamma^-} b\cdot\boldsymbol{n}_K u_h w_h ds\right), \\
l_h(w_h) = &\sum_{e\in\Gamma_h^N}\int_e u^N w_h d\boldsymbol{z} + \sum_{e\in\Gamma_h^D}\int_e u^D\left(\frac{\sigma_e}{h_e}w_h - A\nabla w_h\right) ds \\
&- \sum_{K\in\xi_h}\int_{\partial K^-\cap\Gamma^-} b\cdot\boldsymbol{n}_K u^D w_h ds,
\end{aligned}$$

where u_h^{out} denotes the trace of u_h on an edge e from outside the triangle K. Here, the parameter σ_e is called the penalty parameter, and it should be selected sufficiently large to ensure the coercivity of the bilinear form [24, Sec. 27.1].

The solution of SIPG semi-discretized Heston model (5) is given as

$$u_h(t,\boldsymbol{z}) = \sum_{m=1}^{n_e}\sum_{j=1}^{n_k} u_j^m(t)\varphi_j^m(\boldsymbol{z}), \tag{7}$$

where φ_j^m and u_j^m, $j = 1, \ldots, n_k$, $m = 1, \ldots, n_e$, are the basis functions spanning the space W_h and the unknown coefficients, respectively. The number n_k denotes the local dimension of each dG element with $n_k = (k+1)(k+2)/2$ for 2D problems, and n_e is the number of dG elements (triangles). Substituting (7) into (5) and choosing $v = \varphi_i^k$, $i = 1, \ldots, n_k$, $k = 1, \ldots, n_e$, we obtain the following semi-linear system of ordinary differential equations (ODEs) for the unknown coefficient vector $\boldsymbol{u} := \boldsymbol{u}(t) = (u_1^1(t), \ldots, u_{n_k}^1(t), \ldots, u_1^{n_e}(t), \ldots, u_{n_k}^{n_e}(t))^T \in \mathbb{R}^{\mathcal{N}}$

$$M_h \boldsymbol{u}_t + A_h \boldsymbol{u} = \boldsymbol{l}_h, \tag{8}$$

where M is the mass matrix and A_h is the stiffness matrix, with the entries $(M_h)_{ij} = (\varphi^j, \varphi^i)_\Omega$ and $(A_h)_{ij} = a_h(\cdot; \varphi^j, \varphi^i)$, $1 \leq i, j \leq \mathcal{N} := n_k \times n_e$. For the time discretization, we consider a subdivision of $[0, T]$ into J time intervals $I_n = (t_{n-1}, t_n]$ of length Δt, $n = 1, 2, \ldots, J$, with $t_0 = 0$. Then, the backward Euler solution of the fully discrete formulation of (5) reads as: for $t = 0$ set $u_h^0 \in W_h$ as the projection (orthogonal L^2-projection) of u^0 onto W_h and for $n = 1, 2, \ldots, J$, find $u_h^n := u_h^n(\boldsymbol{z}) \in W_h$ satisfying for all $w_h \in W_h$

$$\int_\Omega \frac{u_h^{n+1} - u_h^n}{\Delta t} w_h d\boldsymbol{z} + a_h(t_{n+1}; u_h^{n+1}, w_h) = l_h(w_h),$$

or in matrix-vector form

$$(M_h + \Delta t A_h)\boldsymbol{u}^{n+1} = M_h \boldsymbol{u}^n + \Delta t \boldsymbol{l}_h^{n+1}. \tag{9}$$

The coefficient matrix $(M_h + \Delta t A_h)$ is factorized by LU decomposition at the initial time step and used in all successive time steps.

3. Reduced order modeling

Both POD and DMD are snapshot-based post-processing algorithms which may be applied equally well to data obtained in simulations or in experiments. The POD is based on the observation that the dynamics of the PDE is optimally contained in a small number of modes computed from a singular value decomposition [17, 30]. After determination of the POD basis by a predetermined cut-off value, the truncated POD modes are used as the basis for Galerkin expansion for the reduced order dynamical system. The DMD can be interpreted as a model order reduction technique like the POD with temporal POD modes [29]. While POD modes are characterized by spatial orthogonality and with multi-frequential temporal content, DMD modes are non-orthogonal but each of them possesses a single temporal frequency. Both methods are conceptually different; POD attempts to build a low-dimensional basis for the solution and DMD attempts to build a low-dimensional basis for the Koopman operator [15]. In the DMD, the eigenfunctions of an unknown linear time-independent operator are approximated, which can be thought of as a finite-dimensional approximation of the infinite-dimensional Koopman operator [15]. The dimensionality reduction occurs through the approximation of the infinite-dimensional set of Koopman

modes with a finite-dimensional set of eigenvectors [29]. Because there are time dynamics associated with each eigenfunction, no analogue of the Galerkin projection is needed to use the DMD modes. DMD is equation free, where the solutions are given in form of Fourier series in space and time. This feature of DMD allows to make future predictions. However the DMD modes are not orthogonal and it requires in general more modes than an equally accurate approximation of the data with POD.

3.1. Proper orthogonal decomposition

To form a reduced order model (ROM) via POD, we construct a low-dimensional ODE system by a Galerkin projection procedure. The full order model (FOM) (8) is of a large dimension $\mathcal{N}$. The ROM of a small dimension $N \ll \mathcal{N}$ for FOM is of the form:

$$\partial_t \boldsymbol{u}^r + \boldsymbol{A}_r \boldsymbol{u}^r = \boldsymbol{l}_r, \tag{10}$$

with the reduced stiffness matrix $\boldsymbol{A}_r = \boldsymbol{U}^T \boldsymbol{A} \boldsymbol{U}$, the reduced vector $\boldsymbol{l}_r = \boldsymbol{U}^T \boldsymbol{l}$, and the unknown vector $\boldsymbol{u}^r \in \mathbb{R}^N$ is the coefficient vector of the reduced solution u_h^r from the N dimensional reduced space $W_{h,r}$ spanned by the reduced basis functions $\{U_i\}_{i=1}^N$. The matrix $\boldsymbol{U} = [\boldsymbol{U}_1, \ldots, \boldsymbol{U}_N] \in \mathbb{R}^{\mathcal{N} \times N}$ is the matrix whose columns $\boldsymbol{U}_i$'s will be called as the reduced basis modes, and they are the coefficient vectors of the reduced basis functions U_i's. Indeed, we have the following relations

$$u_h^r(t, \boldsymbol{z}) = \sum_{i=1}^{N} (\boldsymbol{u}^r)_i(t) U_i(\boldsymbol{z}), \quad U_i(\boldsymbol{z}) = \sum_{j=1}^{\mathcal{N}} \boldsymbol{U}_{j,i} \varphi_j(\boldsymbol{z}), \quad \boldsymbol{u} = \Psi \boldsymbol{u}^r, \tag{11}$$

where $\boldsymbol{u}$ is the coefficient vector of the FOM solution, and $\{\varphi_i\}_{i=1}^{\mathcal{N}}$ are the dG finite elements basis functions, for which then the reduced basis functions U_i's lies in the space W_h and so $W_{h,r} \subset W_h$. The ROM (10) is obtained by the projection of the FOM (8) by the matrix $\boldsymbol{U}$ and by the substitution $\boldsymbol{u} = \boldsymbol{U}\boldsymbol{u}^r$. Another fact with (10) is the M-orthogonality of the reduced modes $\boldsymbol{U}_i$'s, i.e. $\boldsymbol{U}_i^T M \boldsymbol{U}_j = \delta_{ij}$ where δ_{ij} is the Kronecker Delta. For this reason, the reduced mass matrix in (10) is the identity matrix ($\boldsymbol{U}^T M \boldsymbol{U} = \boldsymbol{I}$).

The computation of the reduced modes $\boldsymbol{U}_i$'s are based on the fact that the reduced basis functions U_i's are the solution of the optimization problem [30]

$$\begin{gathered} \min_{U_1,\ldots,U_N} \frac{1}{J} \sum_{j=1}^{J} \left\| u_h^j - \sum_{i=1}^{N} \overbrace{(u_h^j, U_i)_{L^2(\Omega)}}^{(\boldsymbol{u}^r)_i} U_i \right\|_{L^2(\Omega)}^2 \\ \text{subject to } (U_i, U_j)_{L^2(\Omega)} = \boldsymbol{U}_i^T M \boldsymbol{U}_j = \delta_{ij} \ , \ 1 \le i, j \le N, \end{gathered} \tag{12}$$

where $u_h^j := u_h^j(\boldsymbol{z}) \approx u_h(t_j, \boldsymbol{z})$ is the solution through the FOM at $t = t_j$. The minimization problem (12), on the other hand, is equivalent to the eigenvalue problem

$$\widehat{\mathcal{S}}\widehat{\mathcal{S}}^T \widehat{\boldsymbol{U}}_{\cdot,i} = \sigma_i^2 \widehat{\boldsymbol{U}}_{\cdot,i}, \quad i = 1, 2, \ldots, N$$

where $\widehat{\boldsymbol{U}}_{\cdot,i} = R\boldsymbol{U}_{\cdot,i}$, $\widehat{\mathcal{S}} = R\mathcal{S}$, R^T is the Cholesky factor of the mass matrix M, and $\mathcal{S} = [\boldsymbol{u}^1, \ldots, \boldsymbol{u}^J] \in \mathbb{R}^{\mathcal{N}\times J}$ is the snapshot matrix, where $\boldsymbol{u^i} \approx \boldsymbol{u}(t_i)$, $i = 1, 2, \ldots, J$. To have an enough accuracy, the number N of POD modes to be used is selected as the first integer satisfying the relative information content $I(N)$ criteria:

$$I(N) = \frac{\sum_{i=1}^{N} \sigma_i^2}{\sum_{i=1}^{s} \sigma_i^2} \geq 1 - \varepsilon^2,$$

where $I(N)$ represents the energy captured by the first N POD modes for a given tolerance ε, and s is the column rank of the snapshot matrix $\mathcal{S}$.

3.2. Dynamic mode decomposition

We consider the dynamic system on a manifold $\mathcal{M}$

$$\boldsymbol{u}^{n+1} = g(\boldsymbol{u}^n).$$

The linear infinite dimensional Koopman operator [15] maps any function $f : \mathcal{M} \to \mathbb{C}$ into

$$\mathcal{A}f(\boldsymbol{u}^n) = f(g(\boldsymbol{u}^n)).$$

Then, the function $f(\boldsymbol{u}^n)$ can be written as

$$f(\boldsymbol{u}^n) = \sum_{j=1}^{\infty} \alpha_j v_j \lambda_j^n,$$

where the eigenvectors $v_j \in \mathbb{C}$ denote the dynamic modes as Koopman eigenfunctions, $\lambda_j \in \mathbb{C}$ denote the Ritz eigenvalues of the eigenvalue problem $\mathcal{A}v_j = \lambda v_j$ and $\alpha_j \in \mathbb{C}$ denotes the amplitudes of the Koopman modes.

The DMD represents the eigen-decomposition [29] of an approximating linear operator $\mathcal{A}$ corresponding to the Schmidt operator [26], which a is special case of Koopman operator acting on the dynamic variable $\boldsymbol{u}$.

We consider the snapshot matrix $\mathcal{S} = [\boldsymbol{u}^1, \ldots, \boldsymbol{u}^J]$ in $\mathbb{R}^{\mathcal{N}\times J}$ with

$$\mathcal{S}_0 = [\boldsymbol{u}^1, \ldots, \boldsymbol{u}^{J-1}], \quad \mathcal{S}_1 = [\boldsymbol{u}^2, \ldots, \boldsymbol{u}^J],$$

as time discrete solutions of (9).

The DMD is based on the fact that for sufficiently large set of snapshots, the snapshots can be written as

$$\boldsymbol{u}^{n+1} = \mathcal{A}\boldsymbol{u}^n$$

where $\mathcal{A}$ is the Koopman operator. Hence, the snapshots form a Krylov sequence $\mathcal{S}_1 = \{\boldsymbol{u}^1, \mathcal{A}\boldsymbol{u}^1, \mathcal{A}^2\boldsymbol{u}^1, \cdots, \mathcal{A}^{J-1}\boldsymbol{u}^1\}$, where the following snapshots became linearly dependent on the previous ones. The last snapshot $\boldsymbol{u}^J$ is expressed with the error term R as:

$$\boldsymbol{u}^J = c_1\boldsymbol{u}^1 + c_2\boldsymbol{u}^2 + \cdots + c_{J-1}\boldsymbol{u}^{J-1} + R$$

The DMD algorithms are based on the minimization of the norm R. This can be expressed equivalently as $\mathcal{S}_1 \approx \mathcal{A}\mathcal{S}_0$, so that $\tilde{\mathcal{A}}$ is the minimizer of

$$\|\mathcal{S}_1 - \tilde{\mathcal{A}}\mathcal{S}_0\|_F$$

in the Frobenious norm.

Different DMD algorithms are developed for the estimation of Koopman modes, eigenvalues and amplitudes from the given set of snapshots. In this paper we consider the exact DMD algorihm in [29] and a variant of DMD algorithm in [5]. Both algorithms are implemented in the MATLAB Toolbox Koopman mode decomposition [3].

Algorithm 1 Exact DMD Algorithm (Tu et al. [29])

Input: Snapshots $\mathcal{S} = [\boldsymbol{u}^1, \ldots, \boldsymbol{u}^J]$ with $\boldsymbol{u^i} \approx \boldsymbol{u}(t_i)$.
Output: DMD modes Φ^{DMD}.

1: Define the matrices $\mathcal{S}_0 = [\boldsymbol{u}^1, \ldots, \boldsymbol{u}^{J-1}]$ and $\mathcal{S}_1 = [\boldsymbol{u}^2, \ldots, \boldsymbol{u}^J]$.
2: Take SVD of $\mathcal{S}_0 : \mathcal{S}_0 = \boldsymbol{U}\boldsymbol{\Sigma}\boldsymbol{V}^*$.
3: Consider $\tilde{\mathcal{A}} = \boldsymbol{U}^*\mathcal{S}_1\Sigma^{-1}\boldsymbol{V}$.
4: Determine eigenvalues and eigenvectors of $\tilde{\mathcal{A}}W = \Lambda W$
5: Obtain $\Phi^{\mathrm{DMD}} = \mathcal{S}_1\boldsymbol{\Sigma}^{-1}\boldsymbol{V}W$.

Algorithm 2 Variant of DMD Algorithm (Chen et al. [5])

Input: Snapshots $\mathcal{S} = [\boldsymbol{u}^1, \ldots, \boldsymbol{u}^J]$ with $\boldsymbol{u^i} \approx \boldsymbol{u}(t_i)$.
Output: DMD modes Φ^{DMD}.

1: Define the matrices $\mathcal{S}^0 = [\boldsymbol{u}^1, \ldots, \boldsymbol{u}^{J-1}]$ and $\mathcal{S}^1 = [\boldsymbol{u}^2, \ldots, \boldsymbol{u}^J]$.
2: Take SVD of $\mathcal{S}_0^T\mathcal{S}_0 : \mathcal{S}_0^T\mathcal{S}_0 = \boldsymbol{V}\boldsymbol{\Sigma}^2\boldsymbol{V}^*$.
3: Let $\boldsymbol{U} = \mathcal{S}_0\boldsymbol{V}\boldsymbol{\Sigma}^{-1}$.
4: Consider $\tilde{\mathcal{A}} = \boldsymbol{U}^*\mathcal{S}^1\boldsymbol{\Sigma}^{-1}V$
5: Determine eigenvalues and eigenvectors of $\tilde{\mathcal{A}}W = \Lambda W$
6: Obtain $\Phi^{\mathrm{DMD}} = \mathcal{S}^1\boldsymbol{\Sigma}^{-1}\boldsymbol{V}W$.

In POD the modes are ranked by energy level through the POD singular values. There is not such a criteria for ranking the contributions of the different DMD modes. Different criteria are developed depending on what can be considered as important for the models used [28]. The DMD modes can then be selected based on their amplitude or based on their frequency/growth rate. The amplitude criterion is also not perfect because there exist modes with very high amplitudes but which are very fast damped. The selection based on frequency/growth rate has also disadvantages, because it relies on a priori physical knowledge. Additionally, spatial non-orthogonality of the DMD modes may introduce a poor quality of approximation when only a subset of modes with the largest amplitude is retained. Recently several algorithms are developed for selecting optimal amplitudes and extracting the desired frequencies,

spatial profiles using combinatorial search [5] or a gradient-based algorithm or simultaneously search for the low-rank basis [11, 32].

We give here briefly the optimal selection of amplitudes of extracted DMD modes following [14] implemented in the MATLAB Toolbox Koopman mode decomposition [3]. The dynamics of the reduced system in r dimensional subspace is governed by

$$\boldsymbol{u}^{n+1} = \tilde{\mathcal{A}}\boldsymbol{u}^n,$$

where $\tilde{\mathcal{A}} = \boldsymbol{U}^*\mathcal{S}_1\boldsymbol{V}\boldsymbol{\Sigma}^{-1}$ is the reduced matrix obtained from the DMD algorithms Algorithm 1 and Algorithm 2. The reduced solution can be written as linear combination of DMD modes

$$\boldsymbol{u}^r = \sum_{i=1}^{r} \alpha_i \phi_i \lambda_i^k, \quad k \in [0, 1, \ldots, J-1]$$

The unknown optimal amplitudes $\boldsymbol{\alpha} = (\alpha_1, \cdots, \alpha_r)$ are then determined by solving following minimization problem [14]

$$\min_{\alpha} \|\mathcal{S} - \Phi^{\mathrm{DMD}} D_\alpha V_{\mathrm{and}}\|_F^2,$$

where $D_\alpha = \mathrm{diag}(\alpha_1, \ldots, \alpha_r)$ and V_{and} is the Vandermonde matrix $V(\gamma_1, \ldots, \gamma_r)$ with $\gamma_i = \exp(\omega_i t)$, $i = 1, 2, \ldots, k$. Let $P = (W^*W) \circ (\overline{V_{\mathrm{and}} V_{\mathrm{and}}^*})$, $q = \overline{\mathrm{diag}(V_{\mathrm{and}} V \Sigma^* W)}$ where * denotes the conjugate transpose, $\circ$ denotes the elementwise multiplication. Then, $\boldsymbol{\alpha}_{\mathrm{opt}} = P^{-1}q$.

Finally the approximate DMD solution is given as

$$\mathbf{u}^r(t) = \sum_{j=1}^{r} \alpha_j(0)\phi_j(z)\exp(\omega_j t) = \Phi^{\mathrm{DMD}}\mathrm{diag}(\exp(\omega t))\boldsymbol{\alpha}_{Opt}(0),$$

where

$$\Phi^{\mathrm{DMD}} = [\phi_1, \ldots, \phi_k], \quad \boldsymbol{\alpha}_{Opt}(0) = [\alpha_1(0), \ldots, \alpha_k(0)], \quad \omega_j = \log(\lambda_j)/\Delta t.$$

The initial amplitude of the modes are determined by $\boldsymbol{\alpha}_{Opt}(0) = \Phi^\dagger \boldsymbol{u}^1$, where $\Phi^\dagger$ denotes the Moore-Penrose pseudo inverse of the DMD modes Φ^{DMD}.

4. Numerical results

In this section we present numerical results for different options to compare the reduced solutions of POD and DMD with respect to accuracy and speedup. We would like to remark POD and DMD reduced order models are compared in [1] for time-dependent diffusion-convection-reaction equation. It was shown that DMD requires more modes than POD. It is also possible to construct a reduced DMD model using Galerkin projection. But there is no significant difference between the equation free DMD and Galerkin projected reduced model solutions. Therefore we compare the POD reduced model solutions with the equation free DMD solutions for three different options in the following. In all

numerical test we have used linear dG elements in space and backward Euler in time. For computation of the DMD modes we used the MATLAB Toolbox Koopman mode decomposition [3]. The numerical simulations given in this paper are performed on Windows 7 with an Intel Core i7, 2.9Ghz and 8GB RAM using MATLAB R2014a.

4.1. European call option

We impose the initial and boundary conditions in [31]:

$$\begin{aligned} u(\tau, v_{\min}, x) &= Ke^{x-r_f\tau}\Phi(d_+) - Ke^{r_d\tau}\Phi(d_-) \\ u(\tau, v_{\max}, x) &= Ke^{x-r_f\tau} \\ u(\tau, v, x_{\min}) &= \lambda u(\tau, v_{\max}, x_{\min}) + (1-\lambda)u(\tau, v_{\min}, x_{\min}) \\ \frac{\partial}{\partial\nu}u(\tau, v, x_{\max}) &= A\nabla u\cdot\vec{\boldsymbol{n}} = \frac{1}{2}vKe^{x-r_f\tau} \\ u(0, v, x) &= (Ke^x - K)^+ \end{aligned}$$

where $\vec{\boldsymbol{n}}$ is the outward normal vector,

$$d_+ = \frac{x + \left(r_d - r_f + \frac{1}{2}v_{\min}\right)\tau}{\sqrt{v_{\min}\tau}}, \quad d_- = \frac{x + \left(r_d - r_f - \frac{1}{2}v_{\max}\right)\tau}{\sqrt{v_{\max}\tau}}$$

and $\Phi(x)$ is the cumulative distribution function given as

$$\Phi(x) = \frac{1}{2\pi}\int_{-\infty}^{x} e^{-y^2/2}dy.$$

We take the discretization parameters as $\Delta t = 0.01$, $N_x = 96$, and $N_v = 48$ in the domain $[0.0025, 0.5] \times [-5, 5]$. The parameter set for the European call option is taken from [4] with strong negative correlation $\rho = -0.9$.

The relative price and Frobenious errors between the FOM and ROM solutions decay monotonically in Fig. 1 for the POD modes, whereas they reach plateaus and decrease more slowly for the DMD modes. This results from the non-orthogonality of the DMD modes as also observed in [1].

Table 1: Parameter set for the European call option

κ	θ	σ	ρ	r_d	r_f	T	S_0	K	v_0
2.5	0.06	0.4	-0.9	0.0198	0	1	1	1	0.1683

In Fig. 2 the ROM-FOM errors are plotted at the almost same accuracy level for different POD and DMD modes. As expected the POD requires less number of modes than the both DMD algorithms. As can be seen, in the neighborhood of $x = 0$ (i.e $S = K$) and at the boundaries relatively large errors are observed. One of the main reason for this is the initial function $(Ke^x - K)^+$ has a discontinuity in its first derivative at $x = 0$. Hence, we may conclude that the reduced order models could not resolve the full order European call option pricing problem for the at-the-money options.

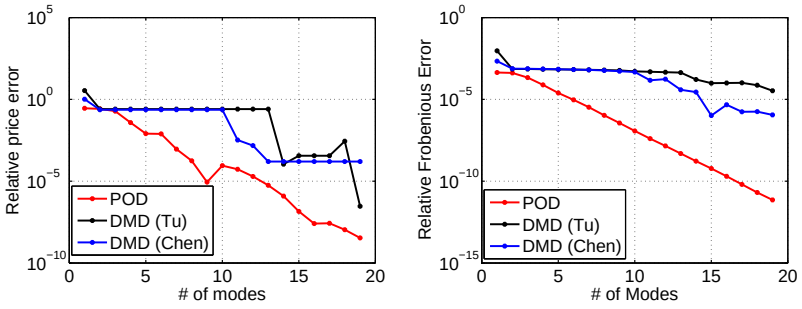

Figure 1: Relative price error for $v_0 = 0.1683$ and $S_0 = 1$ (left), relative Frobenious error (right)

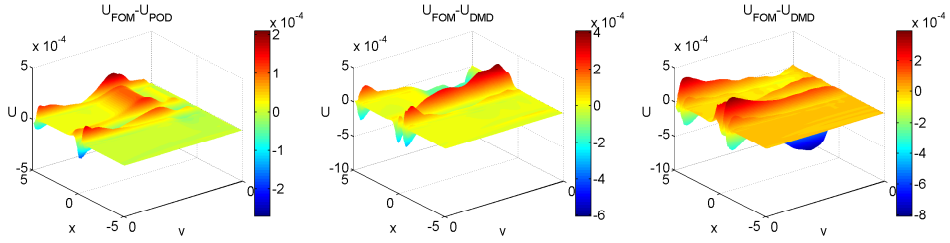

Figure 2: ROM-FOM errors: 8 POD modes (left), 12 DMD (Chen) modes (middle), 18 DMD (Tu) modes function (right).

The performance of the DMD over POD is clearly seen in Table 2. The speed-up factors of both DMD algorithms increases more rapidly than of the POD with increasing number modes. This is due to the fact that the DMD produces equation free solutions, whereas for the POD, for increasing number of modes larger reduced order Galerkin projected ordinary differential equations have to be solved.

4.2. Butterfly spread

The butterfly spread is composed of three call options with different strike prices. Two call options are bought for $K_1 < K_3$, with a strike price K_1 and K_3, and two call options sold with a strike price $K_2 = (K_1 + K_3)/2$. The payoff function is then given by

$$g(v, Ke^x) = (K_2 e^x - K_1)^+ - 2(K_2 e^x - K_2)^+ + (K_2 e^x - K_3)^+,$$

with $x = \log(S/K_2)$. Note that the payoff function (initial data) is non-differentiable at the strike prices K_1, K_2 and K_3.

Let $u(\tau, v, x)$ be the price of a butterfly spread option satisfying Heston's PDE (3) with $x = \log(S/K_2)$. We impose the homogeneous Dirichlet boundary

Table 2: CPU times and speed-up factors of the reduced order solutions

# of modes	CPU time (speed-up)		
	POD	DMD (Tu)	DMD (Chen)
1	0.0331 (577)	0.0219 (872)	0.0202 (946)
2	0.0594 (321)	0.0278 (687)	0.0233 (820)
3	0.0401 (476)	0.0223 (856)	0.0330 (579)
4	0.0590 (324)	0.0223 (856)	0.0224 (853)
5	0.0677 (282)	0.0243 (785)	0.0231 (827)
6	0.0854 (224)	0.0232 (823)	0.0244 (783)
7	0.0821 (233)	0.0241 (793)	0.0228 (838)
8	0.0705 (271)	0.0283 (675)	0.0242 (789)
9	0.0892 (215)	0.0241 (793)	0.0238 (803)
10	0.0958 (200)	0.0247 (773)	0.0242 (789)
11	0.0607 (315)	0.0259 (737)	0.0263 (726)
12	0.0809 (236)	0.0241 (793)	0.0245 (780)
13	0.0959 (199)	0.0249 (767)	0.0243 (786)
14	0.0916 (208)	0.0275 (695)	0.0258 (740)
15	0.1106 (173)	0.0268 (713)	0.0268 (712)
16	0.1031 (185)	0.0295 (647)	0.0367 (520)
17	0.1393 (137)	0.0279 (685)	0.0422 (452)
18	0.1197 (160)	0.0411 (465)	0.0429 (445)
19	0.1248 (153)	0.0468 (408)	0.0421 (453)
	CPU time for full order solution: 19.0996		

conditions in the x-direction and homogeneous Neumann boundary conditions in the v-direction [2]:

$$u(\tau, v, x_{\min}) = 0, \quad u(\tau, v, x_{\max}) = 0,$$

$$\frac{\partial}{\partial v} u(\tau, v_{\min}, x) = 0\ , \quad \frac{\partial}{\partial v} u(\tau, v_{\max}, x) = 0,$$

with an initial condition

$$u(0, v, x) = (K_2 e^x - K_1)^+ - 2(K_2 e^x - K_2)^+ + (K_2 e^x - K_3)^+.$$

The computational domain is taken as for the European call option $(0.0025, 0.5) \times (-5, 5)$. The discretization parameters are taken as $\Delta t = 0.01$, $N_x = 96$, and $N_v = 48$ and $K = 0.5$, $K_1 = 0.1$ and $K_2 = 0.9$.

The parameter set is the same as in [4] with positive correlation $\rho = 0.55$

Table 3: Parameter set for the butterfly spread

κ	θ	σ	ρ	r_d	r_f	T	S_0	v_0
2.5	0.06	0.4	0.55	0.0198	0	1	1	0.1683

The relative price and Frobenious errors in Fig. 3 for the butterfly call option are similar as for the European call option. In this case Tu's DMD algorithm requires less number of DMD modes than the POD at the same level of accuracy, in Fig. 3. Moreover, as described in the European call option case, the reduced order models could not resolve the full order solutions in the neighborhood of $x = 0$.

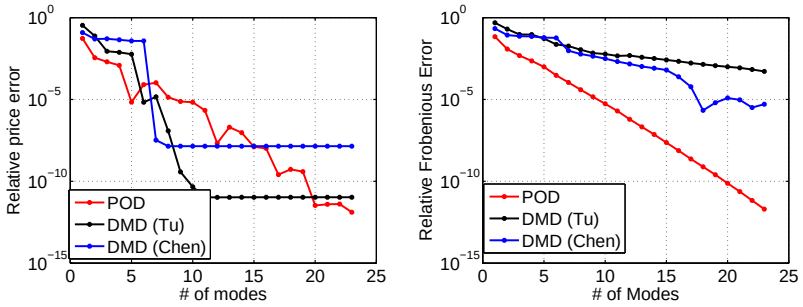

Figure 3: Relative price error for $v_0 = 0.1683$ and $S_0 = 1$ (left), relative Frobenious error (right).

4.3. Digital option

Finally, we consider the digital call options with a discontinuous payoff [9, 18]

$$g(v, Ke^x) = \mathbf{1}_{\{Ke^x > K\}},$$

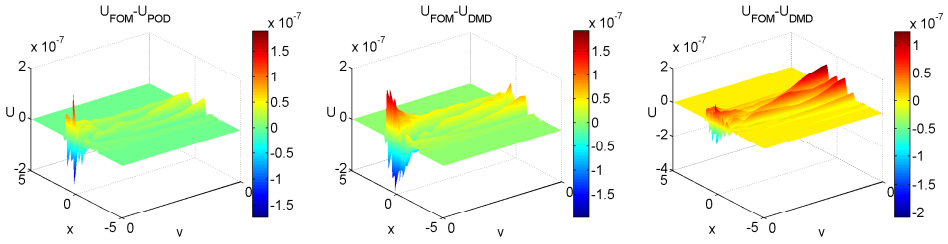

Figure 4: FOM-ROM errors: 14 POD modes (left), 23 DMD (Chen) modes (middle), 8 DMD (Tu) modes function (right).

where K is the strike price of the option, which is treated as a barrier level. Precisely, if the stock price reaches the level K at maturity, then the option will be worthless or it will pay 1 unit of money at time T. The boundary conditions are the same as for the butterfly spread, whereas we now impose an inhomogeneous Dirichlet boundary condition at $x = x_{\max}$ [9]:

$$u(\tau, v, x_{\max}) = e^{x_{\max} - r_f \tau}$$

and an initial condition

$$u(0, v, x) = \mathbf{1}_{\{Ke^x > K\}}.$$

The discretization parameters are $\Delta t = 0.01$, $N_x = 128$, and $N_v = 32$ in the domain $[0.0025, 0.5] \times [-5, 5]$.. The parameters of the Heston's PDE are taken from [31]:.

Table 4: Parameter set for the digital call option

κ	θ	σ	ρ	r_d	r_f	K	T	S_0	v_0
2.5	0.06	0.5	-0.1	log(1.052)	log(1.048)	1	0.25	1	0.05225

The relative price and Frobenious errors and the ROM-FOM errors in Fig. 5 and Fig. 6 show the same behavior as for the European and butterfly spread.

5. Conclusions

The comparison of the POD and DMD reduced order solutions for Heston's PDE for three different options reveals that in general the POD behaves better in terms of the accuracy. But the DMD performs better in terms of the computational cost. A selection between the two methods for a specific option should be based on balancing the accuracy of ROMs and computational cost.

Acknowledgement

This work has been supported by METU BAP-08-11-KB.2014K120600.

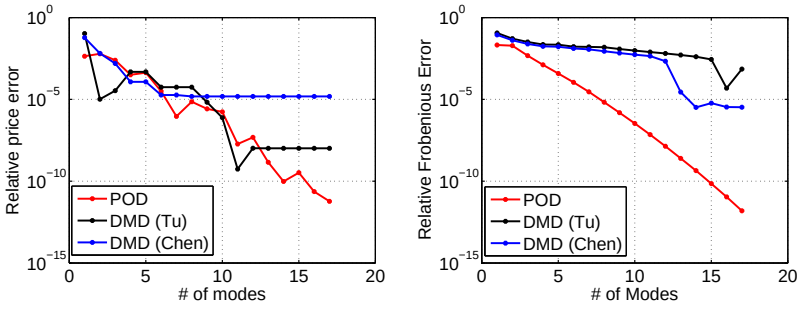

Figure 5: Relative price error for $v_0 = 0.05225$ and $S_0 = 1$ (left), relative Frobenious error (right).

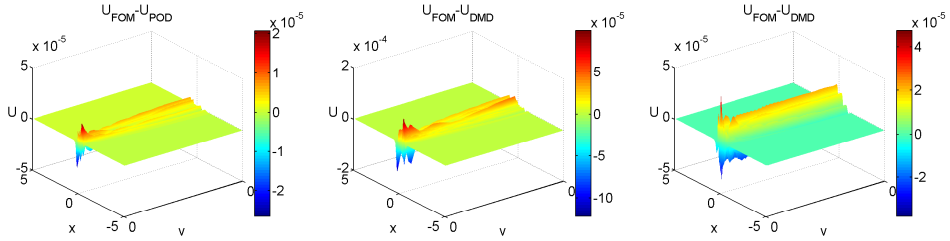

Figure 6: FOM-ROM errors: 9 POD modes (left), 17 DMD (Chen) modes (middle), 9 DMD (Tu) modes (right).

References

[1] Alessandro Alla and J. Nathan Kutz. Nonlinear model order reduction via dynamic mode decomposition. *arXiv:1602.05080*, 2016.

[2] Luca Vincenzo Ballestra and Graziella Pacelli. Pricing European and American options with two stochastic factors: A highly efficient radial basis function approach. *Journal of Economic Dynamics and Control*, 37(6):1142 – 1167, 2013.

[3] Marko Budisic. Matlab toolbox for Koopman mode decomposition. Technical report, Department of Mathematics, University of Wisconsin - Madison, 2015.

[4] O. Burkovska, B. Haasdonk, J. Salomon, and B. Wohlmuth. Reduced basis methods for pricing options with the Black–Scholes and Heston models. *SIAM Journal on Financial Mathematics*, 6(1):685–712, 2015.

[5] Kevin K. Chen, Jonathan H. Tu, and Clarence W. Rowley. Variants of dynamic mode decomposition: Boundary condition, Koopman, and Fourier analyses. *Journal of Nonlinear Science*, 22(6):887–915, 2012.

[6] Rama Cont, Nicolas Lantos, and Olivier Pironneau. A reduced basis for option pricing. *SIAM J. Fin. Math.*, 2(1):287–316, 2011.

[7] Ling-Xiao Cui and Wen Long. Trading strategy based on dynamic mode decomposition: Tested in Chinese stock market. *Physica A: Statistical Mechanics and its Applications*, 461:498 – 508, 2016.

[8] Bertram Düring, Michel Fournié, and Christof Heuer. High-order compact finite difference schemes for option pricing in stochastic volatility models on non-uniform grids. *Journal of Computational and Applied Mathematics*, 271:247 – 266, 2014.

[9] Rachael England. *The use of numerical methods in solving pricing problems for exotic financial derivatives with a stochastic volatility.* PhD thesis, M. Sc. Thesis, University of Reading, 2006.

[10] Jian Gengl. *Calibration of Local Volatility Models and Proper Orthogonal Decomposition Reduced Order Modeling for Stochastic Volatility Models.* PhD thesis, Ph.D. Thesis, Florida State University, 2013.

[11] P. J. Goulart, A. Wynn, and D. Pearson. Optimal mode decomposition for high dimensional systems. In *2012 IEEE 51st IEEE Conference on Decision and Control (CDC)*, pages 4965–4970, 2012.

[12] Steven L. Heston. A closed-form solution for options with stochastic volatility with applications to bond and currency options. *Review of Financial Studies*, 6(2):327–343, 1993.

[13] K. J. In'T Hout and S. Foulon. ADI finite difference schemes for option pricing in the Heston model with correlation. *International Journal of Numerical Analysis and Modeling*, 7(2):303–320, 2010.

[14] Mihailo R. Jovanovi'c, Peter J. Schmid, and Joseph W. Nichols. Sparsity-promoting dynamic mode decomposition. *Physics of Fluids*, 26(2), 2014.

[15] Bernard O Koopman. Hamiltonian systems and transformation in Hilbert space. *Proceedings of the National Academy of Sciences*, 17(5):315–318, 1931.

[16] Sinem Kozpınar, Murat Uzunca, Yeliz Yolcu Okur, and Bülent Karasözen. Option pricing under Heston stochastic volatility model using discontinuous Galerkin finite elements. *arXiv preprint arXiv:1606.08381*, 2016.

[17] K. Kunisch and S. Volkwein. Galerkin proper orthogonal decomposition methods for parabolic problems. *Numerische Mathematik*, 90(1):117–148, 2001.

[18] Vasile L. Lazar. Pricing digital call option in the Heston stochastic volatility model. *Studia Univ. Babeş-Bolyai Math.*, 48(3):83–92, 2003.

[19] Alexander Lipton. *Mathematical methods for foreign exchange: A financial engineer's approach*. World Scientific, 2001.

[20] Jordan Mann and J. Nathan Kutz. Dynamic mode decomposition for financial trading strategies. *Quantitative Finance*, 16(11):1643–1655, 2016.

[21] Antonia Mayerhofer and Karsten Urban. A reduced basis method for parabolic partial differential equations with parameter functions and applications to option pricing. University of Ulm, to appear in Journal of Computational Finance, 2016.

[22] Benjamin Peherstorfer, Pablo Gómez, and Hans-Joachim Bungartz. Reduced models for sparse grid discretizations of the multi-asset Black-Scholes equation. *Advances in Computational Mathematics*, 41(5):1365–1389, 2015.

[23] Olivier Pironneau. Pricing futures by deterministic methods. *Acta Numerica*, 21:577–671, 2012.

[24] B. Rivière. *Discontinuous Galerkin methods for solving elliptic and parabolic equations, Theory and implementation*. SIAM, 2008.

[25] Ekkehard W. Sachs and Matthias Schu. A priori error estimates for reduced order models in finance. *ESAIM:Mathematical Modelling and Numerical Analysis*, 47:449–469, 3 2013.

[26] Peter J. Schmid. Dynamic mode decomposition of numerical and experimental data. *Journal of Fluid Mechanics*, 656:5–28, 2010.

[27] D.Y. Tangman, A. Gopaul, and M. Bhuruth. Numerical pricing of options using high-order compact finite difference schemes. *Journal of Computational and Applied Mathematics*, 218(2):270–280, 2008.

[28] Gilles Tissot, Laurent Cordier, Nicolas Benard, and Bernd R. Noack. Model reduction using dynamic mode decomposition. *Comptes Rendus Mécanique*, 342(6–7):410–416, 2014.

[29] Jonathan H. Tu, Clarence W. Rowley, Dirk M. Luchtenburg, Steven L. Brunton, and J. Nathan Kutz. On dynamic mode decomposition: theory and applications. *J. Comput. Dyn.*, 1(2):391–421, 2014.

[30] S. Volkweinn. Model reduction using proper orthogonal decomposition. Lecture notes, University of Konstanz, 2013.

[31] Gunter Winkler, Thomas Apel, and Uwe Wystup. Valuation of options in Heston's stochastic volatility model using finite element methods. *Foreign Exchange Risk*, pages 283–303, 2001.

[32] A. Wynn, D. Pearson, B. Ganapathisubramani, and P. J. Goulart. Optimal mode decomposition for unsteady flows. *Journal of Fluid Mechanics*, 733:473–503, 2013.